Structural and thermotropic properties of synthetic C16:0 (palmitoyl) ceramide: effect of hydration

Jyotsna Shah, Josephine M. Atienza, Richard I. Duclos, Jr., Anthony V. Rawlings,* Zhengxin Dong,[1] and G. Graham Shipley[2]

Departments of Biophysics and Biochemistry, Center for Advanced Biomedical Research, Boston University School of Medicine, Boston, MA 02118, and Unilever Research U.S. Laboratory,* Edgewater, NJ 07020

Abstract Differential scanning calorimetry (DSC) and X-ray diffraction techniques have been used to investigate the structure and thermotropic properties of synthetic, non-hydroxy fatty acid (16:0) ceramide (NFA(C16)CER) as a function of hydration. Anhydrous NFA(C16)CER shows a single, broad endothermic transition at 95.4°C (ΔH = 10.4 kcal/mol). On hydration, a broad exothermic transition appears at approximately 50–70°C while the main endothermic transition decreases to 90.0°C (ΔH = 13.8 kcal/mol). The enthalpy of the exothermic transition increases with hydration to a maximum value, ΔH = 4.8 kcal/mol. This polymorphic phase behavior depends on the low temperature incubation time and prior cooling rate. X-ray diffraction of fully hydrated NFA(C16)CER at 26°C, shows a well-ordered lamellar phase with a bilayer periodicity d = 46.9 Å. At 68°C, above the first exothermic transition, X-ray diffraction shows again a lamellar phase with reduced bilayer periodicity d = 41.8 Å and an increased number of both lamellar and wide-angle reflections indicative of enhanced layer and chain packing order, respectively. At 90.0°C, above the main transition, the diffraction pattern shows a broad, intense reflection at 29.9 Å and a diffuse reflection at 4.6 Å, indicative of a melted chain phase. On cooling, NFA(C16)CER exhibits polymorphic phase behavior involving the conversion of the melted chain phase to a metastable bilayer phase. On heating, this metastable phase undergoes an exothermic transition to a stable bilayer phase; on further heating, NFA(C16)CER converts endothermically to the melted-chain phase. In addition, low temperature incubation facilitates the conversion of the metastable bilayer phase to the stable bilayer phase. ■ Thus, the chemically simple NFA(C16)CER lacking a polar group exhibits on hydration a complex polymorphic behavior similar to that of more polar sphingolipids such as sphingomyelin, cerebrosides, and sulfatides.—Shah, J., J. M. Atienza, R. I. Duclos, Jr., A. V. Rawlings, Z. Dong, and G. G. Shipley. Structural and thermotropic properties of synthetic C16:0 (palmitoyl) ceramide: effect of hydration. *J. Lipid Res.* 1995. **36:** 1936–1944.

Supplementary key words sphingolipids • cell signaling • second messengers • stratum corneum • X-ray diffraction • scanning calorimetry • bilayers • phase transitions

Most biological membranes contain a heterogeneous mixture of different lipids such as phospholipids, sphin-

golipids, cholesterol, etc. with significant variations in their lipid composition. This membrane lipid composition not only affects the structure of the membrane, it may also affect the properties/function of the membrane. Thus, different tissues have membranes differing in their lipid composition, depending upon the function of the membrane.

Interestingly, the epidermal horny layer (stratum corneum) of mammals, birds, and reptiles contains multiple layers of lamellar membrane sheets occupying the intercellular space between the corneocytes. These membrane lamellae, which contribute significantly to the permeability barrier properties of skin, have an unusual lipid composition (1–4) consisting mainly of ceramides, cholesterol, and free fatty acids. The ceramide component of stratum corneum is chemically heterogeneous due to the sphingosine and N-linked fatty acid moieties differing in chain length, unsaturation, hydroxylation, acylation, etc. (5–9). The structural arrangement and mode of interaction of the lipid components of stratum corneum are not well understood (10, 11). In addition to their role in stratum corneum structure/function, ceramides derived from the enzymatic hydrolysis of sphingomyelin have been shown recently to act as second messengers in cellular signal transduction/cell regulation processes (12–15).

In spite of their specific role in skin and more general role in signal transduction, and in contrast to the lipid components of other membranes, the structure and properties of ceramides have received little attention. A study of the anhydrous N-tetracosanoylphytosphingos-

---

ine indicated that the ceramide can form six crystalline phases depending upon the conditions of crystallization. Only one case was observed in which the two hydrocarbon chains stack parallel in a double layer arrangement in which the longer C24:0 fatty acid chain interdigitates with the sphingosine chain of the other molecule in the opposing leaflet (16, 17). Here, we report on the structure, hydration, and thermotropic properties of a totally synthetic ceramide, NFA(C16)CER, homogeneous in both its sphingosine and fatty acyl (palmitoyl) chains. In an accompanying paper, we describe the properties of two natural ceramide fractions differing in the hydroxylation state of the N-linked fatty acid chain (18).

MATERIALS AND METHODS

D-Galactose, palmitic acid, and N-ethoxycarbonyl-2-ethoxy-1,2-dihydroquinoline (EEDQ) were obtained from Aldrich (Milwaukee, WI). Silica gel 60 was obtained from E. Merck (Darmstadt, Germany). Teflon membranes with 0.5 μm pores were obtained from Alltech (Deerfield, IL).

Synthesis of NFA(C16)CER (Fig. 1)

(2S,3R,4E)-2-Hexadecanoylamino-4-octadecene-1,3-diol (ceramide) was synthesized from (2S,3R,4E)-2-amino-4-octadecene-1,3-diol (sphingosine). The latter was synthesized from D-galactose in seven steps by using the protocol developed by Zimmerman and Schmidt (19).

A solution of sphingosine (160 mg, 0.53 mmol), palmitic acid (190 mg, 0.74 mmol), and EEDQ (262 mg, 1.06 mmol) in dry ethanol (70 mL) was stirred at 50°C for 9 h. The solvent was removed under reduced pressure and the residue was purified by column chromatography on silica gel, eluting first with a) chloroform–methanol 97:3, then with b) chloroform–methanol 95:5. The pure product (237 mg, 83%) was obtained in fraction b as a white solid: m.p. 100.0–102.0°C; R_f 0.46 (chloroform–methanol 9:1); IR (KBr) 3287, 2917, 2849, 1636, 1540, 1489, 1436, 1049 and 960 cm^{-1}; ^{1}H NMR (400 MHz, CDCl$_3$) δ 6.24 (d, 1H), 5.79 (dt, 1H), 5.50 (dd, 1H), 3.96 (dd, 1H), 3.91 (m, 2H), 3.71 (dd, 1H), 2.23 (t, 2H), 2.05 (m, 2H), 1.61 (m, 4H), 1.40–1.21 (m, 44H), 0.89 (t, 6H); ^{13}C NMR (100 MHz, CDCl$_3$) δ 173.9, 134.4, 128.8, 74.8, 62.5, 54.4, 36.8, 32.3, 31.9, 29.7, 29.5, 29.4, 29.3, 29.2, 29.1, 25.8, 22.7, and 14.1.
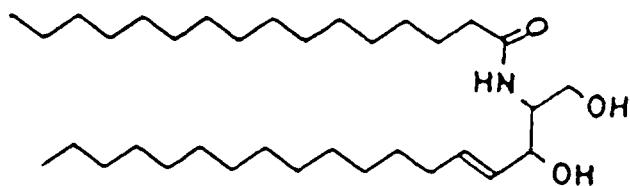

Fig. 1. Structure of N-acylsphingosine (NFA(C16)CER).

Differential scanning calorimetry (DSC)

Hydrated multilamellar suspensions were prepared by a previously described method (20). Distilled, deionized water was added directly, using a Hamilton syringe, to stainless-steel DSC pans containing weighed amounts of NFA(C16)CER. Equilibration was ensured by repeatedly heating and cooling the sample to temperatures above and below the main transition temperature. Samples were stored at -4°C. Calorimetric measurements were made with a Perkin-Elmer (Norwalk, CT) DSC-2 and DSC-7 differential scanning calorimeter at a heating and cooling rate of 5°C/min unless otherwise specified. Data were analyzed by using a Perkin-Elmer Thermal Analysis Data Station (Model 3500) and transition enthalpies were calibrated by comparison with the gallium standard.

X-ray diffraction

Hydrated samples for X-ray diffraction studies were prepared by adding a weighed amount of NFA(C16)CER into a thin-walled capillary (1.0 mm diameter); distilled, deionized water was added to the capillary, the tube centrifuged, weighed, and flame-sealed. To equilibrate, the sample was heated and cooled to temperatures above and below the transition temperature. X-ray diffraction patterns were recorded with photographic film using nickel-filtered Cu Kα radiation (λ = 1.5418 Å) from an Elliot GX-6 rotating anode generator (Elliott Automation, Borehamwood, U.K.). The X-rays were focused into a point source using cameras with toroidal and double-mirror optics. The intensities of the diffraction lines were measured using an Automatic Recording Microdensitometer, Model MK III C. (Joyce-Loebl Ltd., Gateshead, England).

RESULTS

Thermal behavior of fully synthetic ceramide (NFA(C16)CER)

DSC heating scans of NFA(C16)CER at different hydrations are shown in **Fig. 2.** Anhydrous NFA(C16)CER shows (Fig. 2, curve a) a single, broad endothermic transition at 95.4°C (ΔH = 10.9 kcal/mol). With increasing hydration this endothermic transition shifts to lower temperature (Fig. 2, curves b and c); at 9.3% water (Fig. 2, curve d), the transition temperature decreases to 90.2°C (ΔH = 14.0 kcal/mol). Interestingly, a broad exothermic transition starts appearing between 55°C to 70°C (Fig. 2, curve d). On further increasing the hydration, the temperature and enthalpy values of the endothermic transition remain constant at 90.0°C and 13.5 kcal/mol, respectively (Fig. 2, curves d–h). However, the enthalpy of the exothermic transition progressively in-
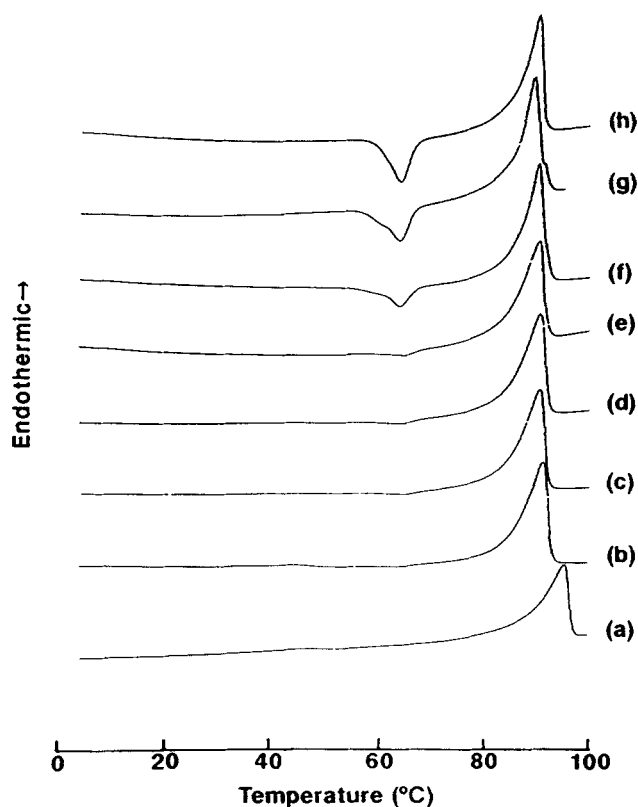
Fig. 2. DSC heating curves; heating rate, 5°C/min. (a) 0 wt.% water; (b) 3.8 wt.% water; (c) 8.0 wt.% water; (d) 9.3 wt.% water; (e) 12.0 wt.% water; (f) 23.1 wt.% water; (g) 34.0 wt.% water; and (h) 74.3 wt.% water.

creases with increasing hydration (Fig. 2, curves d–h). At 74.3% water (Fig. 2, curve h), the heating exotherm occurs at 64.2°C ($\Delta H = 4.8$ kcal/mol).

The cooling scans of both hydrated and anhydrous NFA(C16)CER show complex patterns (data not shown). On cooling, anhydrous NFA(C16)CER shows an exothermic transition at 68°C with a small shoulder on the low temperature side. On increasing the hydration this small peak becomes more prominent. This is accompanied by a reduction in the high temperature peak (data not shown). Fully hydrated NFA(C16)CER exhibits (**Fig. 3,** curves b, f, and h) two exothermic transitions at 65.7°C ($\Delta H = 8.8$ kcal/mol) and 72.4°C ($\Delta H = 1.6$ kcal/mol).
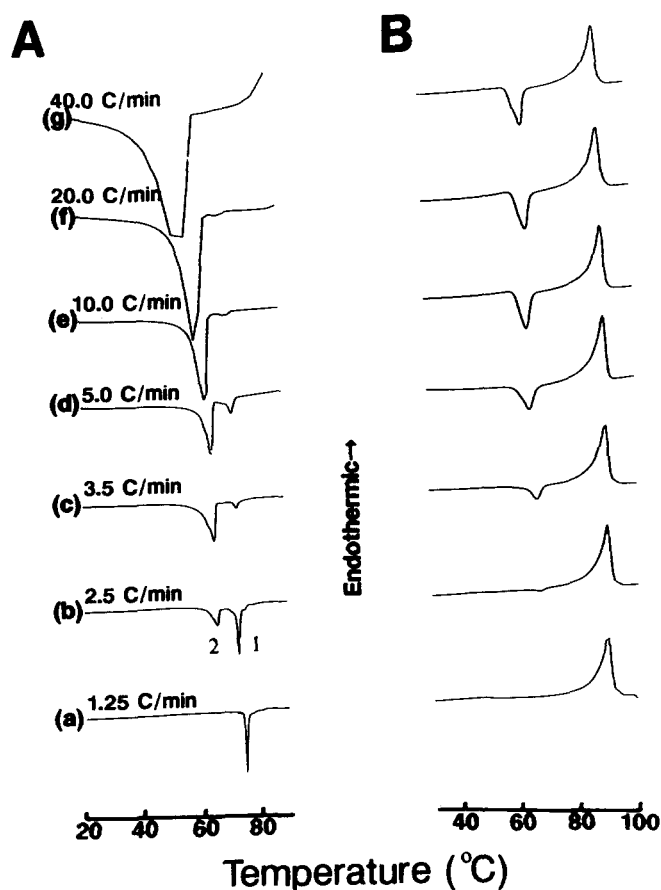
Figure 3 illustrates the polymorphic phase behavior of NFA(C16)CER. The initial DSC heating scan (Fig. 3, curve a) of fully hydrated NFA(C16)CER shows an exotherm at 64.2°C ($\Delta H = 4.8$ kcal/mol), followed by an endotherm at 90.0°C ($\Delta H = 13.5$ kcal/mol). It is proposed that the exotherm is due to the conversion of a less stable (metastable) form to a stable form and the endotherm is due to the lipid chain melting. Immediate cooling to 0°C (Fig. 3, curve b) of NFA-CER results in two exotherms at 65.7°C and 72.4°C. When NFA-CER is heated to 68°C, above the exotherm (Fig. 3, curve c)

and then cooled, no exothermic transition is observed in the cooling run (Fig. 3, curve d). This indicates that the conversion of the metastable phase to the stable phase is an irreversible transition. Subsequent heating to 100°C (Fig. 3, curve e), shows no exothermic transition; only the endothermic transition at 90°C ($\Delta H = 13.5$ kcal/mol) is observed corresponding to the endotherm in the initial heating run (Fig. 3, curve a). On cooling from 100°C to 0°C, the original two exothermic transitions are observed (Fig. 3, curve f; cf 3b). The following heating (Fig. 3, curve g) and cooling (Fig. 3, curve h) scans are identical to the initial heating (Fig. 3, curve a) and cooling (Fig. 3, curve b) scans, respectively.

The effect of different prior cooling rates (1.25 to 40.0°C/min) on the subsequent heating scans of fully hydrated NFA(C16)CER is demonstrated in **Fig. 4.** The cooling runs are recorded at different rates (Fig. 4A) and their subsequent heating runs are recorded at a constant heating rate of 5°C/min (Fig. 4B). The cooling scan at 1.25°C/min (Fig. 4A, curve a), shows only one sharp
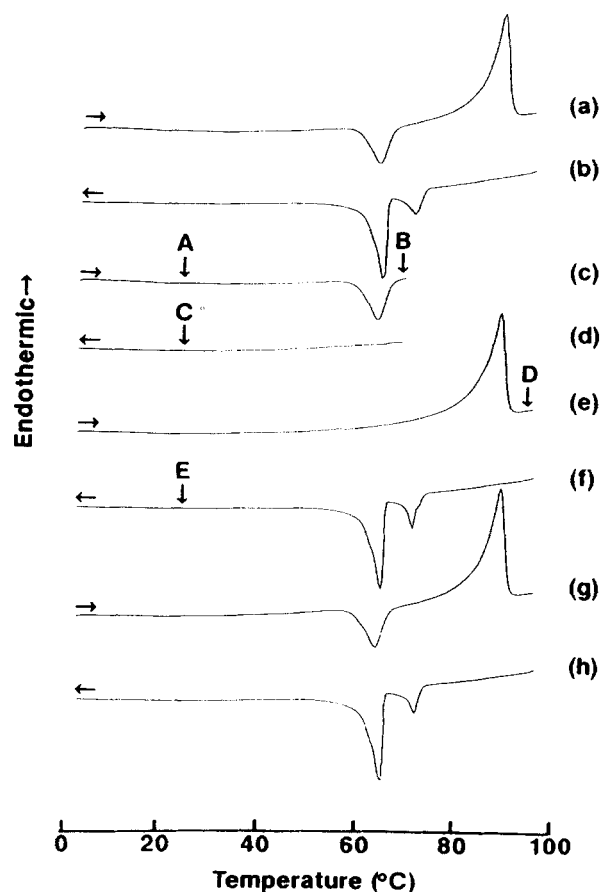
Fig. 3. Successive DSC heating and cooling curves of fully hydrated NFA(C16)CER (74.3% water): (a) heating from 0 to 100°C; (b) corresponding cooling from 100 to 0°C; (c) initial heating to 76.3°C; (d) cooling to 0°C; (e) immediate heating to 100°C; (f) cooling back to 0°C; (g) subsequent heating to 100°C; (h) cooling to 0°C. All curves are scanned at 5°C/min.

A

B

40.0 C/min
(g)

20.0 C/min
(f)

(e) 10.0 C/min

(d) 5.0 C/min

(c) 3.5 C/min

(b) 2.5 C/min

2 | 1

(a) 1.25 C/min

Endothermic→

20 40 60 80   40 60 80 100
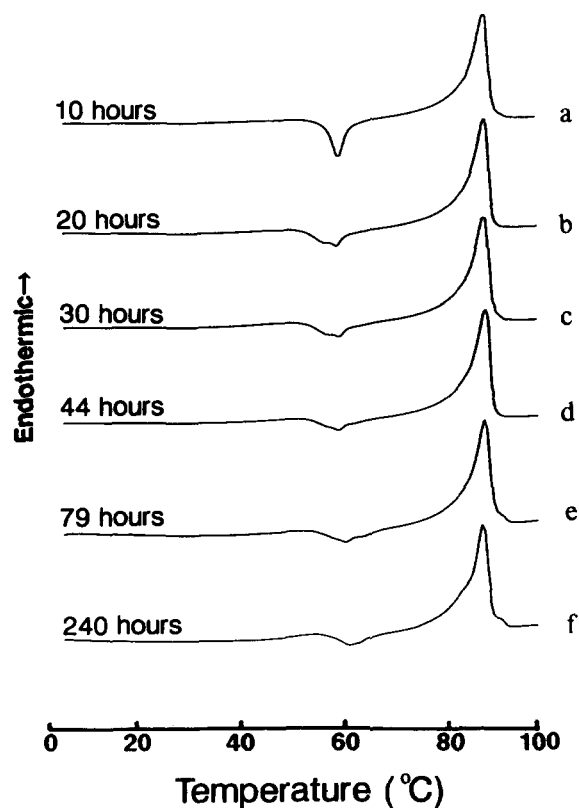
Temperature (°C)

Fig. 4. Effect of cooling rates on the metastable behavior of NFA(C16)CER: DSC cooling curves (panel A) of maximum hydrated NFA(C16)CER at different cooling rates; (a) 1.25°C/min; (b) 2.5°C/min; (c) 3.5°C/min; (d) 5.0°C/min; (e) 10.0°C/min; (f) 20.0°C/min; and (g) 40.0°C/min. Panel B shows the subsequent heating curves at 5°C/min.

exothermic transition at 75.5°C (ΔH = 13.8 kcal/mol). The immediate heating scan (Fig. 4B, curve a) showed only the endothermic transition at 90.0°C (ΔH = 13.5 kcal/mol); no exothermic transition was observed. Increasing the cooling rate to 2.5°C/min (Fig. 4A, curve b), results in decreased enthalpy of the cooling exotherm at 75.5°C (transition 1, ΔH = 7.5 kcal/mol), with a simultaneous appearance of another exotherm at 65.7°C (transition 2, ΔH = 4.5 kcal/mol). The subsequent heating scan (Fig. 4B, curve b) shows a small exotherm in the range 55°C to 70°C, followed by the main endotherm at 90.0°C (ΔH = 13.5 kcal/mol). On further increasing the cooling rate, the enthalpy and temperature of exotherm 1 continuously decrease (limiting Tm = 72.4°C), whereas the enthalpy of exotherm 2 increases (Fig. 4A, curves c–g) reaching a limiting value of 10.7 kcal/mol, at cooling rates higher than 5°C/min. For prior cooling rates greater than 5°C/min, the nature of the heating scans remains the same, i.e., an exotherm

at 64.2°C and an endotherm at 90.0°C (Fig. 4B, curves d–g). The calorimetric data indicate that there is a direct relationship between the exotherm 2 on cooling and the heating exotherm at 64.2°C, i.e., the heating exotherm appears (Fig. 4B, curves b–g) only if cooling exotherm 2 appears (Fig. 4B, curves b–g). These data suggest that the exotherm 1 at 75.5°C is due to conversion of the melted chain phase directly to the stable phase whereas the exotherm 2 may be due to conversion of the melted chain phase to the metastable phase.

To learn more about the metastable and stable phases and to examine whether the metastable phase can convert to the stable phase without heating, fully hydrated NFA(C16)CER is incubated at low temperatures. **Figure 5** shows the effect of different incubation (at 0°C) times on the calorimetric behavior of NFA(C16)CER. On heating the sample, without low temperature incubation, an exothermic transition is observed at 64.2°C (ΔH = 4.8 kcal/mol) followed by an endothermic transition at 90.0°C (see Fig. 2, curve h and Fig. 4B, curve d). Incubation for 10 h at 0°C leads to a decrease in the enthalpy of the exothermic transition from 4.8 kcal/mol to 3.5 kcal/mol, whereas the major endotherm (Tm = 90.0°C, ΔH = 13.5 kcal/mol) remains unaffected by

Endothermic→

10 hours — a

20 hours — b

30 hours — c

44 hours — d

79 hours — e

240 hours — f

0   20   40   60   80   100

Temperature (°C)

Fig. 5. Effect of low temperature incubation time. DSC heating curves of fully hydrated NFA(C16)CER (74.3% water) after incubation for: (a) 10 h; (b) 20 h; (c) 30 h; (d) 44 h; (e) 79 h; (f) 240 h. Heating rate, 5°C/min.

incubation (Fig. 5, curve a). On increasing the incubation time, the enthalpy of the exothermic transition progressively decreases (Fig. 5, curves b–f). After 10 days incubation, the enthalpy of the exotherm is 2.1 kcal/mol (Fig. 5, curve f). The presence of the metastable phase even after 10 days incubation suggests that low temperature incubation (at least, at 0°C) only slowly converts the metastable phase to a stable phase.

X-ray diffraction

To determine the structures of different phases of both anhydrous and hydrated NFA(C16)CER, X-ray diffraction patterns are recorded at different temperatures. X-ray diffraction patterns of anhydrous NFA(C16)CER are recorded below and above its transition temperature. At 26°C (**Fig. 6A**), the low angle region shows sharp reflections corresponding to a lamellar geometry. The lamellar repeat distance, d, is 42.1 Å. The wide angle region is characterized by four sharp reflections at 4.8 Å, 4.3 Å, 4.1 Å, and 3.7 Å (arrow head) indicating an ordered chain packing. On heating anhydrous NFA(C16)CER to 92°C, the low angle region shows a single, broad and intense reflection at 27.5 Å (Fig. 6B). The wide angle region exhibits a wide, diffuse band at 4.7 Å (arrowhead), indicative of melted chains. Cooling of NFA(C16)CER to 26°C results in a diffraction pattern essentially same as Fig. 6A indicating that the original low temperature phase is re-formed and that the chain-melting transition is reversible.

X-ray diffraction patterns of fully hydrated NFA(C16)CER (75 wt % water) at temperatures below

and above the thermal transitions are recorded. The lettered arrows in Fig. 3 correspond to the temperatures at which the X-ray diffraction patterns are recorded (**Fig. 7**). The diffraction pattern at 26°C (Fig. 7A) showed several reflections in the low angle region indexing according to a lamellar geometry; the lamellar repeat distance, d, is 46.9 Å. The wide angle region shows a strong broad reflection centered at 4.1 Å, suggestive of a gel state with hexagonal chain packing.

At 68°C, above the exothermic transition, the X-ray diffraction pattern shows an increased number of low angle reflections indexing to a lamellar repeat distance of 41.8 Å (Fig. 7B). The wide angle region is characterized by several reflections, with the strongest reflections at 4.5 Å, 4.1 Å, 4.0 Å, and 3.8 Å (arrowed). The increased number of reflections indicate that at this temperature (Fig. 7B) NFA(C16)CER is in a more ordered state (in terms of both bilayer stacking and hydrocarbon chain packing) compared to that at 26°C (Fig. 7A). On cooling to 26°C, the diffraction pattern remains unchanged (Fig. 7C), indicating that no phase change occurs during cooling from 68°C to 26°C, consistent with the DSC data (Fig. 3, curve d).

On heating fully hydrated NFA(C16)CER beyond the main endothermic transition, a single, broad intense band at 29.9 Å is observed in the low angle region (Fig. 7D). The wide angle region shows a broad diffuse band at 4.6 Å indicative of a melted chain phase. On cooling to 26°C, (Fig. 3f, point E), as expected NFA(C16)CER gives a diffraction pattern (not shown) essentially identical to the initial diffraction pattern (Fig. 7A), indicating that
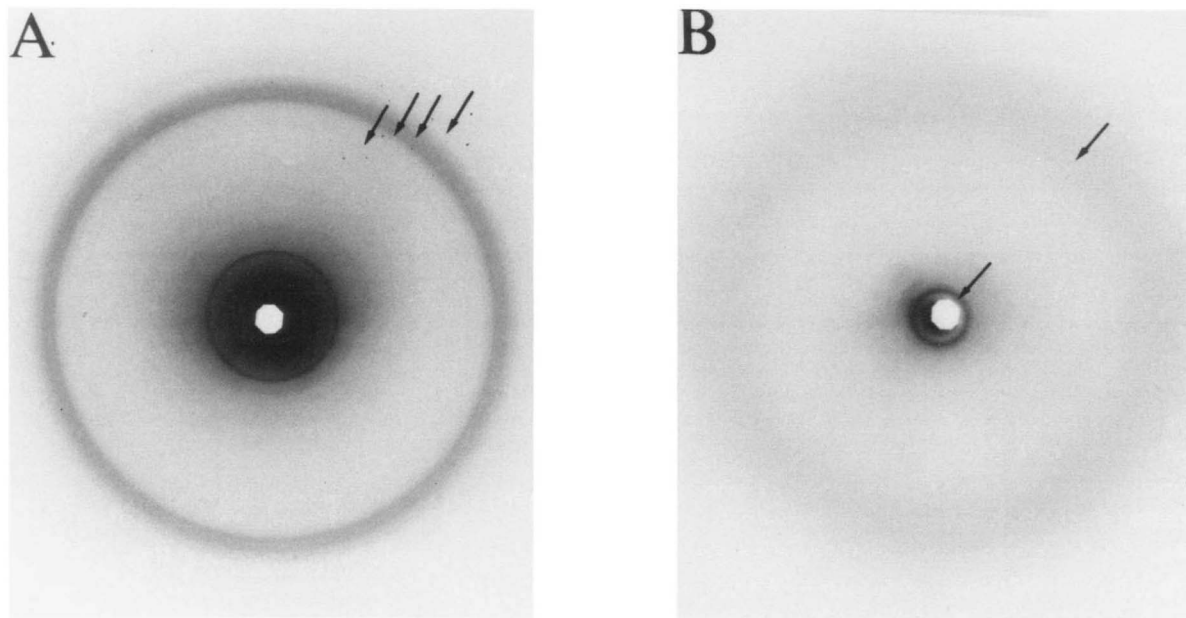

Fig. 6. X-ray diffraction patterns of anhydrous NFA(C16)CER at: (A) 26°C and (B) 95°C.
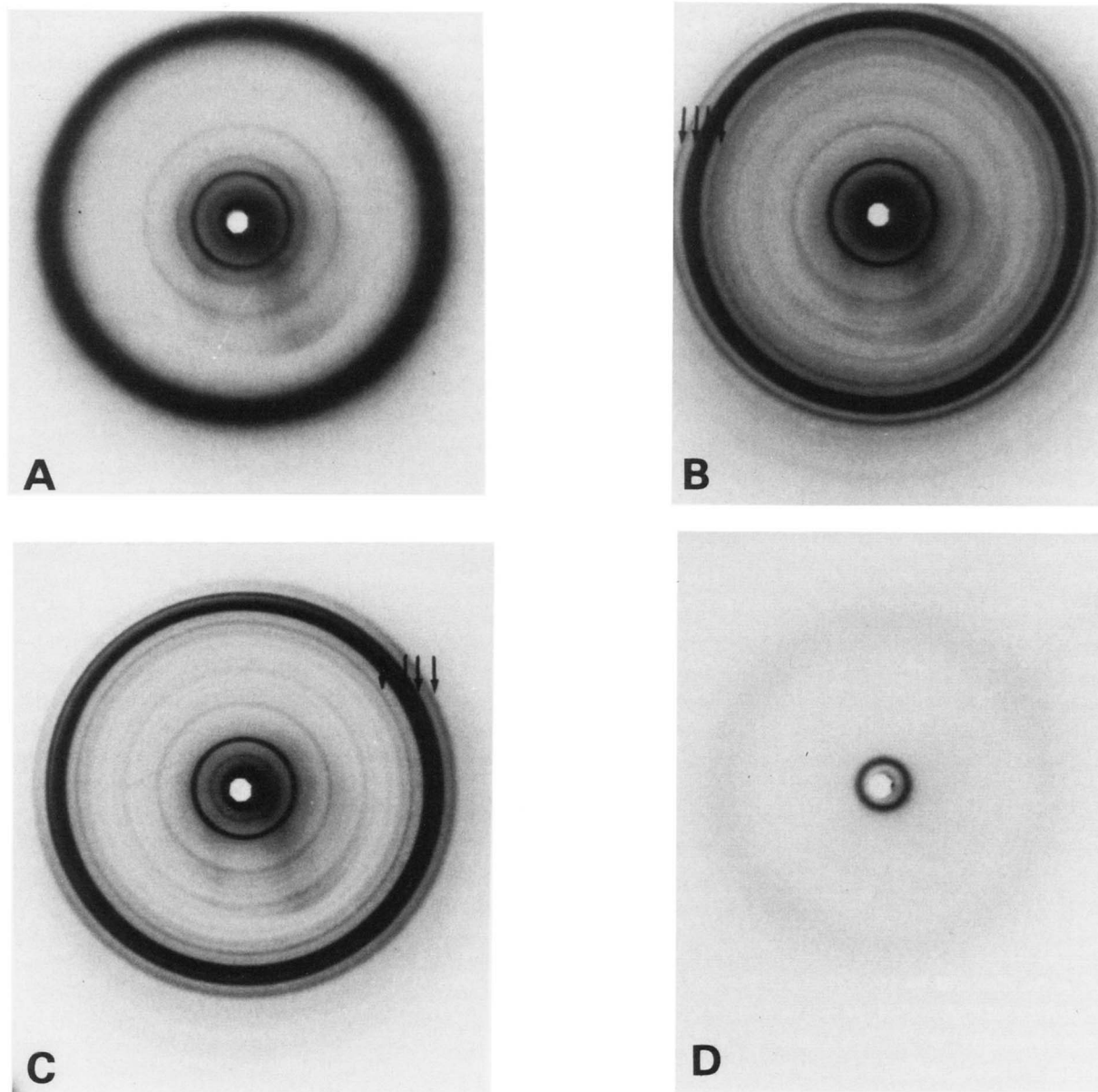
Fig. 7. X-ray diffraction patterns of fully hydrated NFA(C16)CER at: (A) 26°C; (B) 68°C; (C) 26°C, after cooling from 68°C from 26°C; and (D) 91°C, melted-chain phase.

that on cooling the sample from 91°C to 26°C, the initial metastable phase is formed.

DISCUSSION

Anhydrous NFA(C16)CER

The calorimetric data show that on heating anhydrous NFA(C16)CER undergoes a reversible transition at 95.4°C (ΔH = 10.9 kcal/mol). X-ray diffraction of anhydrous NFA(C16)CER at 26°C shows a lamellar bilayer phase with a bilayer spacing of 42.1 Å (Fig. 6A). Wide

angle reflections indicate a highly ordered gel phase with a specific crystalline chain packing. The chains in this conformation are thought to be extended, rigid, in an all-*trans* configuration and are probably involved in specific chain–chain interactions with adjacent ceramide molecules. Above the endothermic transition at 92°C, the low angle region shows a single reflection at 27.5 Å indicative of a disordered phase (Fig. 6B); however, the presence of only one reflection does not allow the type of matrix (lamellar, hexagonal, melt, etc.) to be determined. The wide angle region shows a diffuse band at 4.6 Å, characteristic of a melted-chain phase. Cooling from 92°C to 26°C results in a diffraction

pattern identical to the initial diffraction (Fig. 6A), proving that the transformation of the anhydrous NFA(C16)CER is reversible and involves interconversion of gel/crystalline and melted-chain phases.
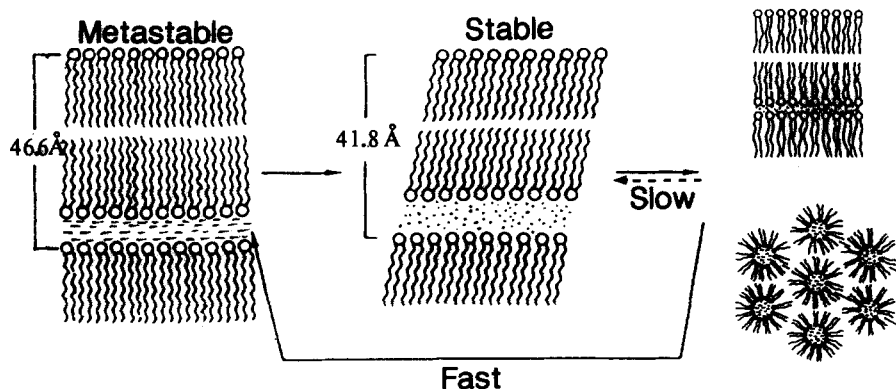
Hydrated NFA(C16)CER

Addition of water causes the appearance of an exotherm at 64.2°C (cf. Fig. 2a and 2h), indicative of conversion of a less stable phase to a more stable phase. The fully hydrated NFA(C16)CER shows two transitions, a low temperature exotherm at 64.2°C and a high temperature endotherm at 90.0°C (Fig. 1, curve h). These data suggest that water of hydration is somehow involved in the formation of the metastable phase.

When fully hydrated (74.3 wt% water) NFA(C16)CER is heated past the exothermic transition (Fig. 3, curve c) and immediately cooled, the cooling run exhibits no transition (Fig. 3, curve d). This indicates that the conversion from the metastable to the stable state is irreversible on cooling. As NFA(C16)CER is already in the stable phase, subsequent heating to 100°C shows no exothermic transition and only the endothermic transition is observed (Fig. 3, curve e). On cooling, the cooling scan (Fig. 3, curve f) is identical to the original cooling scan (Fig. 3, curve b). Subsequent heating (Fig. 3, curve g) and cooling (Fig. 3, curve h) runs produce scans identical to the original heating (Fig. 3, curve a) and cooling (Fig. 3, curve b) scans. This suggests that only when NFA(C16)CER is heated past the endothermic transition and cooled is it able to convert back to the metastable form, and hence, on heating exhibit the reappearance of the exotherm at 64.2°C. This heating exotherm is influenced by low temperature incubation as well as prior cooling rates (see below). On incubation at 0°C, the enthalpy of this exotherm is progressively reduced (Fig. 5), suggesting that during incubation the

metastable phase can slowly convert to the stable phase. Presumably, even longer incubation times at 0°C may lead to complete conversion of the metastable phase to the stable phase.

The effect of prior cooling rate on the subsequent heating scan indicates that the melted-chain phase can be converted to either the metastable phase or the stable phase directly. On cooling at the slowest rate of 1.25°C/min, only exotherm 1 appears at 75.5°C (Fig. 4A, curve a) and the subsequent heating curve shows no exothermic transition; only the chain-melting transition appears (Fig. 4B, curve a). This suggests that on slow cooling the melted-chain phase converts directly to the stable phase. Thus, exothermic transition 1 can be associated with the conversion of the melted-chain phase to the stable phase. Increasing the cooling rate to 2.5°C/min results in a reduction of exotherm 1 and the appearance of exotherm 2 (Fig. 4A, curve b). The subsequent heating scan displays an exothermic transition over the temperature range of 55-70°C (Fig. 4B, curve b). With an increase in the cooling rate, the cooling scans show an increase in the enthalpy of transition 2 (Fig. 4A, curves b-g) and the corresponding heating scans show an increase in the enthalpy of the exotherm at 64.2°C, whereas the endotherm at 90.0°C remains unaffected (Fig. 4B, curves b-g). This indicates a direct correlation between the exotherm 2 and the heating exotherm at 64.2°C (i.e., the heating exotherm at 64.2°C appears only if transition 2 is present in the prior cooling scan). This suggests that on fast cooling, supercooling occurs and more NFA(C16)CER molecules are converted to the metastable phase via transition 2 resulting in an increase in the enthalpy of the subsequent heating exotherm. We, therefore, conclude that transition 1 is due to the conversion of the melted-chain phase to the stable phase and transition 2 is associated with the conversion of the melted-chain phase to the metastable phase. It seems

Fig. 8. Summary of the phase behavior of fully hydrated NFA(C16)CER. Note that the structure of the disordered melted-chain phase of NFA(C16)CER is not known; bilayer and hexagonal structures are shown schematically as possible high temperature phases.

that the kinetic transformation of the melted-chain phase to the stable phase is slow. Slow cooling rates allow NFA(C16)CER to convert exclusively to the stable phase.

Hydrated NFA(C16)CER exhibits slightly different X-ray diffraction patterns compared to the anhydrous form. At low temperature (26°C), the low angle reflections show a lamellar bilayer phase with a lamellar period of 46.9 Å which is ~5 Å greater than its anhydrous form (d = 42.1 Å). This is probably due to the water molecules incorporated between adjacent lipid layers. Increasing the temperature past the exothermic transition shows an increased number of reflections in both the low and wide angle regions, indicating an increase in both lamellar stacking order and chain packing order. This indicates that during the heating, exothermic transition NFA(C16)CER converts from a metastable gel phase to a stable phase with more ordered crystalline chain packing and is consistent with the calorimetric data (see above). For this stable phase, the reflections in the low angle region correspond to a lamellar bilayer gel phase with a reduced (compared to the low temperature phase) bilayer repeat distance of 41.8 Å. This decrease in the bilayer periodicity may be due to the tilting of the hydrocarbon chains with respect to the bilayer normal. On cooling from 68°C to 26°C, the diffraction pattern does not change (Fig. 7C), supporting the DSC evidence that on cooling no phase transition is observed. Above the endothermic transition in the chain-melted state, the low angle region shows a single reflection indicating a highly disordered phase of, as yet, undefined structure.

Figure 8 summarizes the structural and thermotropic behavior of fully hydrated NFA(C16)CER. At low temperatures after equilibration or fast cooling from 92°C, a well-ordered metastable bilayer gel phase exists with a bilayer periodicity of 46.9 Å. On increasing the temperature an exothermic transition occurs at 64.2°C to form a stable bilayer phase with crystalline chain packing and a reduced bilayer periodicity of 41.8 Å. This decrease in periodicity may be due to the increased chain tilting with respect to the bilayer normal and/or dehydration. On further increasing the temperature, this crystalline phase converts into a disordered melted-chain phase. On "fast" cooling, the melted-chain phase converts back to the metastable phase, whereas on "slow" cooling NFA(C16)CER can convert directly to the stable phase.

This type of thermotropic behavior with exothermic transitions between metastable and stable bilayer states has also been observed for other sphingolipids like sphingomyelin (21), cerebrosides (22–24), and cerebroside sulfate (25–27). For cerebrosides this behavior was attributed to hydrogen bonding via the glycosyl hydroxyls and amide group (28) and water–sugar interactions (22). As ceramides do not have a sugar moiety, the polymorphic behavior and metastability can, per-

haps, be attributed to the hydrogen bonding of the hydroxyl groups of the sphingosine to the amide group of adjacent molecules and to the lateral chain interactions. The transformation of ceramides from the liquid–crystalline to the stable phase may be a two-step process involving the initial ordering of the hydrocarbon chains to form the metastable phase followed by the rearrangement of the hydrogen bonding network and/or chain packing resulting in the formation of the stable phase.

REFERENCES

1. Gray, G. M., and H. J. Yardley. 1975. Different populations of pig epidermal cells: isolation and lipid composition. *J. Lipid Res.* **16:** 441–447.
2. Gray, G. M., and H. J. Yardley. 1975. Lipid composition of cells isolated from pig, human and rat epidermis. *J. Lipid Res.* **16:** 434–440.
3. Gray, G. M., and R. J. White. 1978. Glycosphingolipid and ceramides in human and pig epidermis. *J. Invest. Dermatol.* **70:** 336–341.
4. Elias, P. M., and G. K. Menon. 1991. Structural and lipid biochemical correlates of the epidermal permeability barrier. *Adv. Lipid Res.* **24:** 1–26.
5. Wertz, P. W., and D. T. Downing. 1983. Acylglucosyl-ceramides of pig epidermis: structure determination. *J. Lipid Res.* **23:** 753–758.
6. Wertz, P. W., and D. T. Downing. 1983. Ceramides of pig epidermis: structure determination. *J. Lipid Res.* **24:** 759–765.
7. Wertz, P. W., M. C. Miethke, S. A. Long, J. S. Strauss, and J. T. Downing. 1985. The composition of the ceramides from human stratum corneum and from comedones. *J. Invest. Dermatol.* **84:** 410–412.
8. Long, S. A., P. W. Wertz, J. S. Strauss, and D. T. Downing. 1985. Human stratum corneum polar lipids and desquamation. *Arch. Dermatol. Res.* **277:** 284–287.
9. Schurer, N. Y., and P. M. Elias. 1991. The biochemistry and function of stratum corneum lipids. *Adv. Lipid Res.* **24:** 27–56.
10. White, S. H., D. Mirezovsky, and G. I. King. 1988. Structure of lamellar lipid domains and corneocyte envelopes of murine stratum corneum. An X-ray diffraction study. *Biochemistry.* **27:** 3725–3732.
11. Bouwstra, J. A., G. S. Gooris, J. A. Van Der Spek, and W. Bras. 1991. Structural investigations of human stratum corneum by small-angle X-ray scattering. *J. Invest. Dermatol.* **97:** 1005–1012.
12. Merrill, A. H., Jr. 1992. Ceramide: a new "lipid messenger"? *Nutr. Rev.* **50:** 78–80.
13. Hannun, Y. A., and R. M. Bell. 1993. The sphingomyelin cycle: a prototype sphingolipid signalling pathway. *Adv. Lipid Res.* **25:** 27–41.

14. Hannun, Y. A. 1994. The sphingomyelin cycle and second messenger function of ceramide. *J. Biol. Chem.* **269:** 3125–3128.
15. Hannun, Y. A., and C. M. Linardic. 1994. Sphingolipid breakdown products: anti-proliferative and tumor-suppressor lipids. *Biochim. Biophys. Acta.* **1154:** 223–236.
16. Dahlen, B., and I. Pascher. 1972. Molecular arrangements in sphingolipids. Crystal structure of N-tetracosanoylphytosphingosine. *Acta Crystallogr.* **B28:** 2396–2404.
17. Pascher, I., M. Lundmark, P. G. Nyholm, and S. Sundell. 1992. Crystal structure of membrane lipids. *Biochim. Biophys. Acta.* **1113:** 339–373.
18. Shah, J., J. M. Atienza, A. V. Rawlings, and G. G. Shipley. 1995. Structural and thermotropic properties of hydroxy and non-hydroxy fatty acid ceramides. *J. Lipid Res.* **36,** 1945–1955.
19. Zimmerman, P., and R. R. Schmidt. 1988. Synthese von erythro-sphingosinen uber die azidoderivate. *Liebigs Ann. Chem.* 663–667.
20. Shah, J., P. K. Sripada, and G. G. Shipley. 1990. Structure and properties of mixed-chain phosphatidylcholine bilayers. *Biochemistry.* **29:** 4254–4262.
21. Estep, T. N., W. I. Calhoun, Y. Barenholz, R. L. Biltonen, G. G. Shipley, and T. E. Thompson. 1980. Evidence for metastability in stearoylsphingomyelin bilayers. *Biochemistry.* **19:** 20–25.
22. Ruocco, M., J., D. Atkinson, D. M. Small, R. P. Skarjune, E. Oldfield, and G. G. Shipley. 1981. X-ray diffraction and calorimetric study of anhydrous and hydrated N-palmitoylgalactosylsphingosine (cerebroside). *Biochemistry.* **20:** 5957–5966.
23. Curatolo, W. 1982. Thermal behavior of fractionated and unfractionated bovine brain cerebrosides. *Biochemistry.* **21:** 1761–1772.
24. Freire, E., D. Bach, M. Correa-Freire, I. Miller, and Y. Barenholz. 1980. Calorimetric investigation of the complex phase behavior of glucocerebroside dispersions. *Biochemistry.* **19:** 3662–3670.
25. Koshy, K. M., and J. M. Boggs. 1983. Partial synthesis and physical properties of cerebroside sulfate containing palmitic acid or alpha-hydroxy palmitic acid. *Chem. Phys. Lipids.* **34:** 41–53.
26. Boggs, J. M., K. M. Koshy, and G. Rangaraj. 1984. Effect of fatty acid chain length, fatty acid hydroxylation, and various cations on phase behavior of synthetic cerebroside sulfate. *Chem. Phys. Lipids.* **36:** 65–89.
27. Boggs, J. M., K. M. Koshy, and G. Rangaraj. 1988. Influence of structural modifications on the phase behavior of semi-synthetic cerebroside sulfate. *Biochim. Biophys. Acta.* **938:** 361–372.
28. Curatolo, W., and F. B. Jungalwala. 1985. Phase behavior of galactocerebrosides from bovine brain. *Biochemistry.* **24:** 6608–6613.